

A SCHRÖDINGER-BASED DISPERSIVE REGULARIZATION APPROACH FOR NUMERICAL SIMULATION OF ONE-DIMENSIONAL SHALLOW WATER EQUATIONS

GUOSHENG FU AND CHUN LIU

ABSTRACT. We propose a novel dispersive regularization framework for the numerical simulation of the one-dimensional shallow water equations (SWE). The classical hyperbolic system is regularized by a third-order dispersive term in the momentum equation, which renders the system equivalent, via the Madelung transform, to a defocusing cubic nonlinear Schrödinger equation with a drift term induced by bottom topography.

Instead of solving the shallow water equations directly, we solve the associated Schrödinger equation and recover the hydrodynamic variables through a simple postprocessing procedure. This approach transforms the original nonlinear hyperbolic system into a semilinear complex-valued equation, which can be efficiently approximated using a Strang time-splitting method combined with a spectral element discretization in space.

Numerical experiments demonstrate that, in subcritical regimes without shock formation, the Schrödinger regularization provides an $O(\varepsilon)$ approximation to the classical shallow water solution, where ε denotes the regularization parameter. Importantly, we observe that this convergence behavior persists even in the presence of moving wetting–drying interfaces, where vacuum states emerge and standard shallow water solvers often encounter difficulties. These results suggest that the Schrödinger-based formulation offers a robust and promising alternative framework for the numerical simulation of shallow water flows with dry states.

1. INTRODUCTION AND MOTIVATION

The shallow water equations (SWE) are a fundamental model for free-surface flows arising in river hydraulics, coastal engineering, and geophysical fluid dynamics [24]. Despite their apparent simplicity, the numerical simulation of SWE remains challenging, particularly in the presence of wetting–drying interfaces and vacuum states, where the water depth vanishes and the equations degenerate.

A wide range of numerical methods has been developed for SWE, including finite volume, finite difference, and discontinuous Galerkin (DG) schemes. To handle dry states, these methods typically rely on carefully designed positivity-preserving limiters, hydrostatic reconstructions, and ad hoc regularizations of the velocity field [3, 7, 18, 26, 27]. While such approaches are effective in many practical applications, they often entail substantial algorithmic complexity and problem-dependent tuning, and the robust treatment of moving wetting–drying fronts remains a delicate issue.

An alternative modeling approach is the use of *dispersive regularizations* of hyperbolic systems. Rather than introducing artificial viscosity, dispersive terms are incorporated in a way that preserves conservation laws and, in many cases, an underlying Hamiltonian or variational structure. Such dispersive mechanisms arise naturally in the hydrodynamic formulation of the nonlinear Schrödinger equation and in Euler–Korteweg-type models [9, 20]. Through the Madelung transform, solutions of the Schrödinger equation can be interpreted in hydrodynamic variables, leading to a dispersively regularized Euler-type system involving a quantum

2020 *Mathematics Subject Classification.* 65M70, 65N35, 76B15, 35Q55.

Key words and phrases. Shallow water equations; Dispersive regularization; Nonlinear Schrödinger equation; Madelung transform; Wetting and drying; Spectral element method; Strang splitting.

G. Fu's research is partially supported by NSF grant DMS-2410741. Part of this research was performed while G. Fu was visiting the Institute for Mathematical and Statistical Innovation (IMSI), which is supported by the National Science Foundation (Grant No. DMS-2425650). C. Liu's research is partially supported by NSF grant DMS-2216926 and DMS-2410742.

(or Bohm) potential. These equations have been extensively studied in the context of the semi-classical limit of Schrödinger dynamics [6, 8, 13], with the primary objective of understanding the behavior and limiting properties of the Schrödinger equation itself, rather than serving as numerical regularizations of classical hyperbolic conservation laws.

In this work, we build on these ideas and exploit the dispersive structure induced by the Madelung transform as a numerical approximation framework for the one-dimensional shallow water equations. Specifically, we introduce a dispersive regularization of SWE that is equivalent to a defocusing cubic nonlinear Schrödinger equation with a drift term induced by bottom topography. Rather than solving the shallow water equations directly, we solve the associated Schrödinger equation and recover the physical variables through a simple postprocessing procedure. This reformulation converts the original nonlinear hyperbolic system into a semilinear complex-valued equation, which is well suited for efficient numerical approximation using time-splitting methods and high-order spatial discretizations.

From a modeling and numerical perspective, the Schrödinger formulation has several appealing features. First, the water height is represented as the squared modulus of the wave function, which guarantees non-negativity and naturally accommodates vacuum states. Second, the resulting semilinear structure allows for efficient numerical schemes based on Strang splitting, in which the dispersive and potential subproblems can be treated separately. Finally, the dispersive regularization provides a controlled small-parameter approximation to the dispersionless shallow water equations in regimes where the solution remains smooth.

The main contributions of this paper can be summarized as follows:

- We introduce a dispersive regularization of the one-dimensional shallow water equations that is equivalent to a defocusing cubic nonlinear Schrödinger equation with drift induced by bottom topography.
- We present an energetic variational (EnVarA) interpretation of the regularized formulation, clarifying the origin of the dispersive term from an energy-based viewpoint.
- We develop an efficient numerical method based on spectral element discretization in space and Strang splitting in time, leading to linear constant-coefficient subproblems in the dispersive step and analytic, pointwise updates in the potential step.
- Through a series of numerical experiments, we demonstrate that the proposed approach yields $\mathcal{O}(\varepsilon)$ accuracy in subcritical and shock-free regimes, including challenging scenarios involving moving wetting-drying interfaces and vacuum formation.

The remainder of the paper is organized as follows. In Section 2, we introduce the dispersive regularization and its equivalence to a nonlinear Schrödinger equation, and describe the numerical discretization. Section 3 presents numerical results illustrating the strengths and limitations of the proposed approach. Concluding remarks and directions for future work are given in Section 4.

2. SCHRÖDINGER REGULARIZATION AND NUMERICAL METHOD

2.1. Shallow Water Equations. We consider the one-dimensional shallow water equations with bottom topography $b(x)$,

$$h_t + (hu)_x = 0, \quad (1a)$$

$$(hu)_t + \left(hu^2 + \frac{1}{2}gh^2 \right)_x = -ghb_x, \quad (1b)$$

where $g > 0$ denotes the gravitational constant, $h(x, t) \geq 0$ is the water depth, and $u(x, t)$ is the depth-averaged velocity.

2.2. Energetic variational approach and dispersive regularization. The shallow water equations can be interpreted within the framework of the energetic variational approach (EnVarA), which provides a systematic way to derive governing equations from energy functionals

by combining the least action principle with force balance laws; see, e.g., [12, 19]. This perspective is particularly useful for elucidating the conservative structure of the equations and for incorporating additional physical effects through modifications of the energy.

For the one-dimensional shallow water equations, the total energy is given by

$$\mathcal{E}(h, u) = \mathcal{K}(h, u) + \mathcal{F}(h) = \int_{\Omega} \frac{1}{2} h |u|^2 dx + \int_{\Omega} \left(\frac{1}{2} gh^2 + gb(x)h \right) dx,$$

where \mathcal{K} denotes the kinetic energy, \mathcal{F} the potential energy associated with gravity and bottom topography, and Ω is the spatial domain. The kinematic constraint relating the water height and the velocity is the mass conservation law (1a). In the absence of dissipation, smooth solutions satisfy the energy conservation law

$$\frac{d}{dt} \mathcal{E}(h, u) = 0. \quad (2)$$

Within EnVarA, the conservative dynamics are derived by introducing a flow map $x = x(X, t)$ satisfying

$$\partial_t x(X, t) = u(x(X, t), t), \quad x(X, 0) = X,$$

together with mass conservation. In one space dimension, mass conservation is equivalently expressed in Lagrangian form as

$$h(x(X, t), t) x_X(X, t) = h_0(X),$$

or, in Eulerian form, as (1a).

Consider the kinetic-energy action functional in Lagrangian coordinates,

$$\mathcal{A}[x] = \int_0^T \int_{\Omega_0} \frac{1}{2} h_0(X) |\partial_t x(X, t)|^2 dX dt.$$

A standard variation $x \mapsto x + \eta$ with $\eta(\cdot, 0) = \eta(\cdot, T) = 0$ yields

$$\delta \mathcal{A} = - \int_0^T \int_{\Omega_0} h_0(X) \partial_{tt} x(X, t) \eta(X, t) dX dt.$$

Transforming back to Eulerian variables using $h_0(X) dX = h(x, t) dx$ and the identity $\partial_{tt} x(X, t) = u_t(x, t) + u(x, t)u_x(x, t)$, we obtain the inertial force

$$f_{\text{inertial}} = \frac{\delta \mathcal{A}}{\delta x} = -h(u_t + uu_x).$$

We next derive the conservative force induced by the potential energy

$$\mathcal{F}(h) = \int_{\Omega} \left(\frac{1}{2} gh^2 + gb(x)h \right) dx.$$

Let $\xi(x, t)$ be the Eulerian displacement associated with the perturbed flow. Mass conservation implies the transport identity

$$\delta h = -\partial_x(h \xi). \quad (3)$$

Using $\delta \mathcal{F} = \int (\delta \mathcal{F} / \delta h) \delta h dx$ with

$$\frac{\delta \mathcal{F}}{\delta h} = g(h + b),$$

we obtain

$$\delta \mathcal{F} = - \int_{\Omega} g(h + b) \partial_x(h \xi) dx = \int_{\Omega} h \partial_x(g(h + b)) \xi dx,$$

where the last step follows from integration by parts (assuming periodic boundary conditions or vanishing boundary terms). Hence,

$$f_{\text{conservative}} = \frac{\delta \mathcal{F}}{\delta x} = h \partial_x(g(h + b)).$$

The EnVarA force balance

$$\frac{\delta \mathcal{A}}{\delta x} = \frac{\delta \mathcal{F}}{\delta x},$$

together with mass conservation (1a), recovers the momentum equation (1b).

A central advantage of EnVarA is that additional conservative effects can be incorporated by augmenting the energy functional. To introduce dispersion, we add the Fisher-information energy

$$\mathcal{F}_{\text{disp}}(h) = \frac{\varepsilon^2}{2} \int_{\Omega} |(\sqrt{h})_x|^2 dx = \frac{\varepsilon^2}{8} \int_{\Omega} \frac{h_x^2}{h} dx, \quad (4)$$

where $\varepsilon > 0$ is the regularization parameter. Energies of the form (4) also appear in a different context in Schrödinger bridge and entropic optimal transport problems, where the Fisher-information term arises naturally from stochastic perturbations of the continuity equation and can be interpreted as a noise-induced regularization; see, e.g., [10, 17].

A direct variational calculation yields the associated chemical potential

$$\frac{\delta \mathcal{F}_{\text{disp}}}{\delta h} = -\frac{\varepsilon^2}{2} \frac{(\sqrt{h})_{xx}}{\sqrt{h}} =: \mu, \quad (5)$$

which is the *quantum (Bohm) potential* in the Madelung literature [9, 20]. Using the same transport identity (3), the dispersive contribution to the conservative force is

$$f_{\text{disp}} = \frac{\delta \mathcal{F}_{\text{disp}}}{\delta x} = h \mu_x.$$

Combining the forces gives the regularized momentum balance

$$h(u_t + uu_x) + h \partial_x(g(h + b)) + h \mu_x = 0. \quad (6)$$

The regularized system (1a) and (6) is Hamiltonian and satisfies the modified energy conservation law

$$\frac{d}{dt} (\mathcal{E}(h, u) + \mathcal{F}_{\text{disp}}(h)) = 0,$$

for smooth solutions and under appropriate boundary conditions.

2.3. Dispersive Regularization and the Nonlinear Schrödinger Equation. The dispersively regularized shallow water system derived in the previous subsection, cf. (1a) and (6), admits an equivalent formulation in terms of a nonlinear Schrödinger equation. This equivalence follows from the classical Madelung transform and highlights that the Fisher-information regularization naturally induces a Schrödinger-type structure.

Specifically, assuming the existence of a real-valued velocity potential ϕ such that $u = \phi_x$, and introducing the complex-valued wave function

$$\psi(x, t) = \sqrt{h(x, t)} \exp\left(\frac{i}{\varepsilon} \phi(x, t)\right),$$

it can be shown that the regularized shallow water equations (1a)–(6) are formally equivalent to the defocusing nonlinear Schrödinger equation (NLS)

$$i\varepsilon \psi_t = -\frac{\varepsilon^2}{2} \psi_{xx} + g|\psi|^2 \psi + gb(x)\psi, \quad (7)$$

where the bottom topography enters as an external potential.

The hydrodynamic variables, namely the water height h and the discharge $q = hu$, are recovered from the wave function ψ through the relations

$$h = |\psi|^2, \quad q = \varepsilon \text{Im}(\bar{\psi} \psi_x). \quad (8)$$

The main objective of this work is to numerically solve the nonlinear Schrödinger equation (7) in the small- ε regime and to use the resulting Madelung variables (8) as an approximation to the solution of the original dispersionless shallow water equations (1).

2.4. Semiclassical Limit and Approximation Regimes. The convergence of solutions of the nonlinear Schrödinger equation (7) in the limit $\varepsilon \rightarrow 0$ has been extensively studied in the context of the semiclassical (or zero-dispersion) limit of NLS; see, for example, [8, 9, 13]. In regimes where the limiting solution of the dispersionless shallow water equations (1a)–(1b) remains smooth and the water height h stays uniformly bounded away from zero, it is well known that the Madelung variables (8) associated with the Schrödinger solution converge locally in time to the corresponding strong solution of the shallow water system.

When the dispersionless shallow water equations develop shocks (e.g., in supercritical regimes), strong pointwise convergence is no longer expected. In this case, solutions of the nonlinear Schrödinger equation typically develop rapidly oscillatory wave trains, known as *dispersive shock waves*, with characteristic wavelength of order $O(\varepsilon)$; see, for instance, [11, 15, 16]. The limiting behavior in this regime is commonly described in a weak or averaged sense using Whitham modulation theory [25]. As a consequence, the nonlinear Schrödinger equation is not expected to provide a pointwise approximation of entropy solutions of the shallow water equations after shock formation (often referred to as gradient catastrophe in the semiclassical NLS literature).

The primary focus of the present work is the numerical reliability of the Schrödinger-based approximation in shock-free regimes where wetting–drying interfaces may occur. The convergence theory in the presence of moving wetting–drying fronts remains far less developed due to the loss of smoothness near vacuum boundaries. Our numerical results indicate that, even in this setting, the nonlinear Schrödinger equation provides accurate approximations of the shallow water solution. A salient feature of the proposed approach is that no ad hoc wetting–drying treatment is required: the reconstructed water height $h = |\psi|^2$ is guaranteed to remain non-negative throughout the computation.

2.5. Numerical Scheme for NLS. The numerical approximation of NLS (7) has been extensively studied. A wide variety of discretization strategies have been proposed, including finite difference methods, finite element/discontinuous Galerkin methods, and spectral or pseudo-spectral methods; see, for example, [1, 4–6, 14].

In the semiclassical regime $\varepsilon \ll 1$, the numerical approximation of (7) becomes particularly challenging due to the presence of highly oscillatory solutions. It is well known that spatial mesh sizes and time step sizes must be chosen in relation to the small parameter ε in order to accurately resolve the oscillatory behavior; see, e.g., [5, 21]. Failure to respect these resolution constraints typically leads to loss of accuracy or spurious numerical artifacts.

In this work, we adopt a spectral element method for the spatial discretization of (7). For the temporal discretization, we employ a second-order Strang splitting scheme; see [6], in which the linear dispersive operator is separated from the nonlinear potential terms. This strategy yields an efficient algorithm: the dispersive substep reduces to the solution of a constant-coefficient linear problem, while the nonlinear potential substep can be solved exactly and locally at each degree of freedom. As a result, the overall scheme is computationally efficient and particularly well suited for simulations in the small- ε regime.

For simplicity, we consider the one-dimensional spatial domain $\Omega = [-L, L]$. Let $\Omega_h = \{T\}$ be a conforming partition of Ω into elements. We define the complex-valued spectral element space

$$V_h^k = \{v \in H^1(\Omega) : v|_T \in \mathcal{P}_k(T), \forall T \in \Omega_h\}, \quad (9)$$

where $k \geq 1$ denotes the polynomial degree. As is standard in spectral element methods, Gauss–Lobatto interpolation points and basis functions are employed in the implementation.

We assume periodic boundary conditions for (7) (other boundary conditions will be discussed in the next subsection) and define the periodic finite element space

$$V_{h,\text{per}}^k := \{v \in V_h^k : v(-L) = v(L)\}.$$

The spatial discretization of (7) then reads: find $\psi_h(t) \in V_{h,\text{per}}^k$ such that

$$(i\varepsilon\psi_{h,t}, \phi_h)_h - \frac{\varepsilon^2}{2}(\psi_{h,x}, \phi_{h,x})_h = (g|\psi_h|^2\psi_h + gb(x)\psi_h, \phi_h)_h, \quad \forall \phi_h \in V_{h,\text{per}}^k. \quad (10)$$

Here $(\cdot, \cdot)_h$ denotes the discrete L^2 inner product obtained by approximating integrals over each element using the $(k+1)$ -point Gauss–Lobatto quadrature rule. This choice results in a diagonal mass matrix.

For the temporal discretization, we employ a second-order Strang splitting method, in which (7) is decomposed into linear dispersive and nonlinear potential subproblems:

$$i\varepsilon\psi_t = -\frac{\varepsilon^2}{2}\psi_{xx}, \quad (11a)$$

$$i\varepsilon\psi_t = g|\psi|^2\psi + gb(x)\psi. \quad (11b)$$

Starting from a known approximation $\psi_h^n \approx \psi(t_n)$, the Strang splitting algorithm with time step size $\Delta t > 0$ proceeds as follows.

Step 1: Half-step nonlinear potential update. We evolve (11b) over the half time interval $[t_n, t_n + \frac{1}{2}\Delta t]$, with initial condition $\psi_h(t_n) = \psi_h^n$. The semi-discrete formulation reads

$$(i\varepsilon\psi_{h,t}, \phi_h)_h = (g|\psi_h|^2\psi_h + gb(x)\psi_h, \phi_h)_h, \quad \forall \phi_h \in V_{h,\text{per}}^k. \quad (12)$$

Due to the use of Gauss–Lobatto basis functions and quadrature, this system decouples at each degree of freedom, leading to the following nodal ODEs:

$$i\varepsilon \frac{d}{dt} \psi_h(x_j, t) = g(|\psi_h(x_j, t)|^2 + b(x_j))\psi_h(x_j, t), \quad \forall x_j \in X_h, \quad (13)$$

where $X_h = \{x_j\}$ denotes the set of all Gauss–Lobatto quadrature nodes on Ω_h .

Multiplying (13) by $\overline{\psi_h}(x_j, t)$ and extracting the imaginary part shows that $\frac{d}{dt}|\psi_h(x_j, t)|^2 = 0$ for all $x_j \in X_h$. Consequently, the nonlinear potential step preserves $|\psi_h|$ pointwise and can be integrated exactly:

$$\psi_h(x_j, t) = \exp\left(-\frac{i}{\varepsilon}g(|\psi_h(x_j, t_n)|^2 + b(x_j))(t - t_n)\right)\psi_h(x_j, t_n), \quad x_j \in X_h. \quad (14)$$

We denote the resulting solution at $t_n + \frac{1}{2}\Delta t$ by $\psi_h^{n,*} = \psi_h(t_n + \frac{1}{2}\Delta t)$.

Step 2: Full-step linear dispersive update. We next evolve the linear dispersive subproblem (11a) over the full time step Δt , starting from $\psi_h^{n,*}$. A Crank–Nicolson discretization in time yields

$$\left(i\varepsilon \frac{\psi_h^{n+1,*} - \psi_h^{n,*}}{\Delta t}, \phi_h\right)_h - \frac{\varepsilon^2}{2}((\psi_{h,x})^{n+1/2,*}, \phi_{h,x})_h = 0, \quad \forall \phi_h \in V_{h,\text{per}}^k, \quad (15)$$

where

$$\psi_h^{n+1/2,*} = \frac{1}{2}(\psi_h^{n+1,*} + \psi_h^{n,*}).$$

This step requires the solution of a linear system with constant coefficients. In our implementation, the resulting system is solved efficiently using a preconditioned MINRES iterative solver equipped with a spectrally equivalent block-diagonal preconditioner.

Step 3: Half-step nonlinear potential update. Finally, we apply the nonlinear potential step (11b) again over the half interval $[t_n + \frac{1}{2}\Delta t, t_{n+1}]$, yielding

$$\psi_h(x_j, t) = \exp\left(-\frac{i}{\varepsilon}g(|\psi_h^{n+1,*}(x_j)|^2 + b(x_j))(t - t_n - \frac{1}{2}\Delta t)\right)\psi_h^{n+1,*}(x_j), \quad x_j \in X_h. \quad (16)$$

The final approximation is then defined by $\psi_h^{n+1}(x) = \psi_h(x, t_{n+1}) \in V_{h,\text{per}}^k$.

2.6. Boundary Conditions. We conclude this section with a discussion of the treatment of far-field boundary conditions for the nonlinear Schrödinger equation (7). Many problems of interest are naturally posed on the whole space \mathbb{R} , whereas numerical simulations must be carried out on a bounded computational domain. It is therefore necessary to impose suitable artificial boundary conditions on a truncated domain that minimize spurious reflections and accurately represent the far-field behavior of the solution.

In this work, we employ a sponge-layer (or absorbing-layer) approach to model far-field boundary conditions. The idea is to introduce a damping region near the artificial boundaries of the computational domain, where outgoing waves are gradually attenuated before reaching the

boundary. This strategy allows waves generated in the interior to exit the computational domain with minimal reflection and provides a simple and robust treatment of far-field boundaries for the Schrödinger equation.

Specifically, we extend the spatial domain from $\Omega = [-L, L]$ to $\Omega_{\text{ext}} = [-(L + \ell), L + \ell]$, where $\ell > 0$ denotes the width of the sponge layer. The regions $[-(L + \ell), -L] \cup [L, L + \ell]$ constitute the sponge layers. We then augment (7) with a complex absorbing potential (CAP) term, leading to the modified equation

$$i\varepsilon\psi_t = -\frac{\varepsilon^2}{2}\psi_{xx} + g|\psi|^2\psi + gb(x)\psi - i\sigma(x)\psi. \quad (17)$$

Here $\sigma(x) \geq 0$ is a spatially dependent damping function supported only within the sponge layers.

In our implementation, $\sigma(x)$ is chosen using a quintic smoothstep ramp,

$$\sigma(x) = \sigma_{\max} \left[6 \left(\frac{|x| - L}{\ell} \right)^5 - 15 \left(\frac{|x| - L}{\ell} \right)^4 + 10 \left(\frac{|x| - L}{\ell} \right)^3 \right], \quad L < |x| < L + \ell, \quad (18)$$

and $\sigma(x) = 0$ for $|x| \leq L$.

The sponge-layer thickness is taken as

$$\ell = N \frac{2\pi\varepsilon}{|\omega|}, \quad \text{with } N = 16, \quad (19)$$

where ω denotes the dominant outgoing wave number. The maximum damping strength is chosen as

$$\sigma_{\max} = -\frac{2\varepsilon|\omega|}{\ell} \log(10^{-6}), \quad (20)$$

corresponding to a target amplitude reduction of 10^{-6} across the sponge layer.

With the sponge layer in place, we impose homogeneous Neumann boundary conditions $\psi_x = 0$ at the boundaries of the extended domain, i.e., at $|x| = L + \ell$. Since outgoing waves are strongly attenuated within the sponge region, this simple boundary condition introduces negligible reflection into the interior computational domain.

To incorporate the sponge layers into the Strang splitting scheme described in the previous subsection, we proceed as follows. The linear dispersive substep (11a) is unchanged. On the interior region $[-L, L]$, where $\sigma(x) = 0$, the nonlinear potential updates remain identical to (14)–(16). The only modification occurs in the sponge layers, where the complex absorbing potential term $-i\sigma(x)\psi$ introduces an additional damping effect. At the Gauss–Lobatto nodes $x_j \in X_h$, the half-step update (14) in the sponge layer takes the closed form

$$\psi_h(x_j) \mapsto \exp\left(-\frac{i}{\varepsilon}g(|\psi_h(x_j)|^2 + b(x_j))\frac{\Delta t}{2}\right) \exp\left(-\frac{\sigma(x_j)\Delta t}{\varepsilon}\frac{\Delta t}{2}\right) \psi_h(x_j), \quad x_j \in X_h. \quad (21)$$

The same modification is applied in the final nonlinear half-step of the Strang splitting scheme.

3. NUMERICAL RESULTS

We present a series of numerical experiments to validate the proposed Schrödinger-based approximation framework for the one-dimensional shallow water equations. All simulations are performed using the lowest-order spectral element discretization with polynomial degree $k = 1$. A uniform spatial mesh with resolution $\Delta x = 0.05\varepsilon$ is used, and the time step size is chosen as $\Delta t = \Delta x$. The gravitational constant is fixed to $g = 1$ throughout. In the results presented below, we take $\varepsilon = 0.01$, which is representative of the small-dispersion regime considered in this work. All numerical simulations are carried out using the MFEM finite element library [2].

3.1. Riemann-Type Test Problems. In this subsection, we consider several representative Riemann problems for the shallow water equations (1). In all cases, the initial data consist of two constant states separated at $x = 0$,

$$(h(x, 0), u(x, 0)) = \begin{cases} (h_L, u_L), & x < 0, \\ (h_R, u_R), & x > 0, \end{cases} \quad (22)$$

with flat bottom topography $b(x) = 0$. Depending on the choice of left and right states, the corresponding exact solutions may involve rarefaction waves, vacuum states, or shock formation [24].

To initialize the nonlinear Schrödinger equation (7), we employ a uniform regularization strategy for all Riemann problems. The initial water height is approximated by the smooth profile

$$h_0(x) = \frac{h_L + h_R}{2} + \frac{h_R - h_L}{2} \tanh(x/\delta), \quad \delta = 1.2 \varepsilon, \quad (23)$$

and the initial wave function is defined as

$$\psi(x, 0) = \sqrt{h_0(x)} \exp\left(\frac{i}{\varepsilon} \phi_0(x)\right). \quad (24)$$

The phase function $\phi_0(x)$ is chosen so that its derivative provides a smooth approximation of the Riemann initial velocity,

$$\phi'_0(x) = \frac{u_R + u_L}{2} + \frac{u_R - u_L}{2} \tanh\left(\frac{x}{\delta}\right). \quad (25)$$

Here we take

$$\phi_0(x) = \frac{u_R + u_L}{2} x + \frac{u_R - u_L}{2} \delta \left(|x/\delta| + \log(1 + e^{-2|x|/\delta}) \right).$$

Unless otherwise stated, computations are performed on $\Omega = [-2, 2]$ with homogeneous Neumann boundary conditions and final time $t = 0.6$. We now discuss three representative choices of Riemann data.

3.1.1. Dam-Break Problem with a Dry Bed. We first consider a dam-break problem with a dry bed to the right, corresponding to

$$(h_L, u_L) = (1.0, 0), \quad (h_R, u_R) = (0, 0).$$

The exact solution consists of a single rarefaction wave, with water height given by [24]

$$h(x, t) = \begin{cases} 1, & x/t < -1, \\ \frac{(2 - x/t)^2}{9}, & -1 \leq x/t \leq 2, \\ 0, & x/t > 2. \end{cases}$$

Figure 1 displays the computed Schrödinger wave function together with the reconstructed water height and discharge at the final time $t = 0.6$. As expected in the small- ε regime, the real and imaginary parts of the wave function exhibit rapidly oscillatory behavior with characteristic frequency of order $\mathcal{O}(1/\varepsilon)$. Interestingly, these oscillations largely cancel when the solution is expressed in terms of the reconstructed hydrodynamic variables. In particular, both the water height and the discharge remain smooth across the wet-dry interface and agree very well with the corresponding *dispersionless shallow water Riemann solution* in this region.

Small-amplitude oscillations of order $\mathcal{O}(\varepsilon)$ are also observed near the head of the left-going rarefaction wave. Such oscillations are consistent with dispersive effects introduced by the Schrödinger regularization and diminish as ε decreases. Overall, the results demonstrate that, despite the highly oscillatory nature of the underlying wave function, the Schrödinger-based approach provides an accurate approximation of the shallow water solution in the shock-free regime, including in the presence of a moving wet-dry interface.

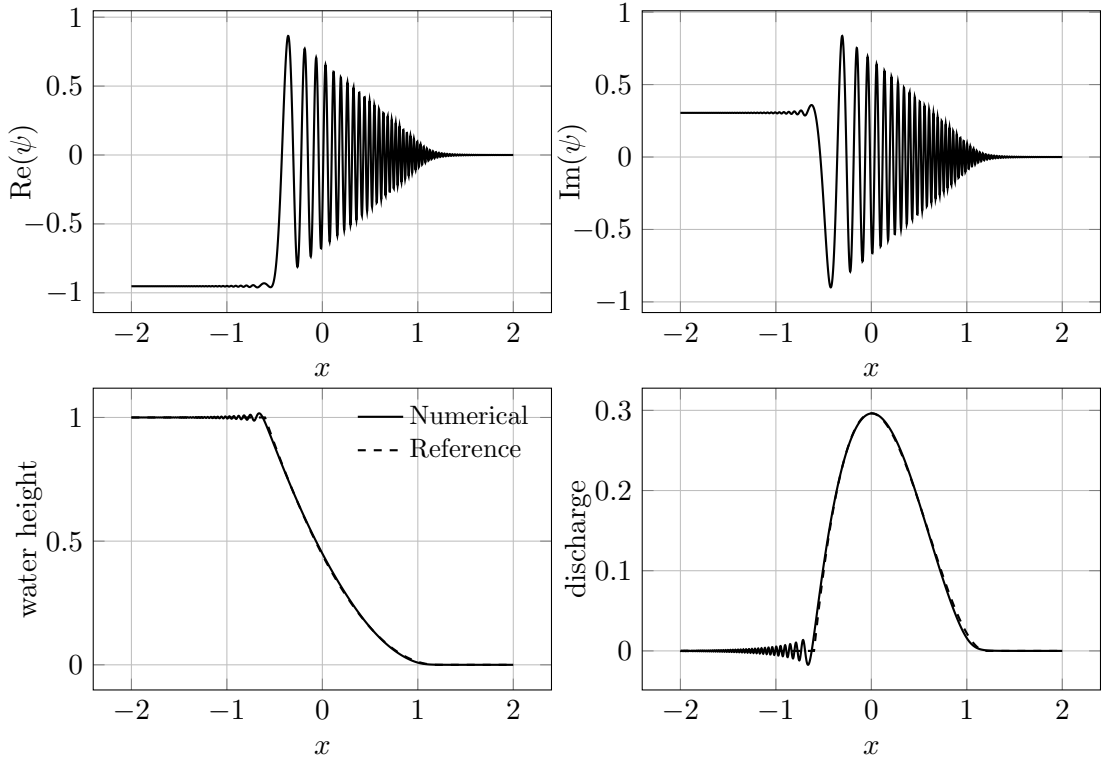


FIGURE 1. Numerical solution of the dam-break problem with a dry bed described in Subsection 3.1.1. The top row shows the real and imaginary parts of the Schrödinger wave function ψ . The bottom row displays the reconstructed hydrodynamic variables, namely the water height $h = |\psi|^2$ and the discharge $q = \varepsilon \text{Im}(\bar{\psi} \psi_x)$. The numerical solutions are compared with the corresponding dispersionless shallow water Riemann solution.

3.1.2. *Dam-Break Problem with a Wet Bed.* We next consider a dam-break Riemann problem with a wet bed on the right, which leads to shock formation. The initial left and right states are given by

$$(h_L, u_L) = (1.0, 0), \quad (h_R, u_R) = (0.2, 0).$$

For this configuration, the exact solution of the dispersionless shallow water equations consists of a left-going rarefaction wave followed by a right-going shock [24].

Figure 2 shows the numerical solution of the dam-break problem with a wet bed at the final time $t = 0.6$. As in the previous example, the top row displays the real and imaginary parts of the Schrödinger wave function, which exhibit rapidly oscillatory behavior in the small- ε regime. The bottom row presents the reconstructed hydrodynamic variables, namely the water height and the discharge, together with the corresponding dispersionless shallow water Riemann solution.

In the region associated with the left-going rarefaction wave, the reconstructed water height and discharge agree well with the dispersionless shallow water solution. In this regime, the oscillations present in the wave function largely cancel when expressed in terms of the hydrodynamic variables, and the Schrödinger-based approximation provides a reasonable representation of the underlying shallow water dynamics.

In contrast, near the right-going shock, the Schrödinger solution no longer approximates the dispersionless shock profile. Instead of converging to a monotone entropy shock as in the shallow water equations, the solution develops a rapidly oscillatory structure characteristic of a dispersive shock wave. These oscillations persist in the reconstructed water height and discharge and do not vanish as ε decreases.

This behavior reflects a fundamental limitation of the present approach: the nonlinear Schrödinger regularization replaces gradient catastrophe in the dispersionless shallow water

equations by dispersive shock waves rather than classical entropy shocks. Consequently, while the Schrödinger-based formulation performs well in shock-free regimes, it is not suitable for approximating shallow water solutions in the presence of shock formation.

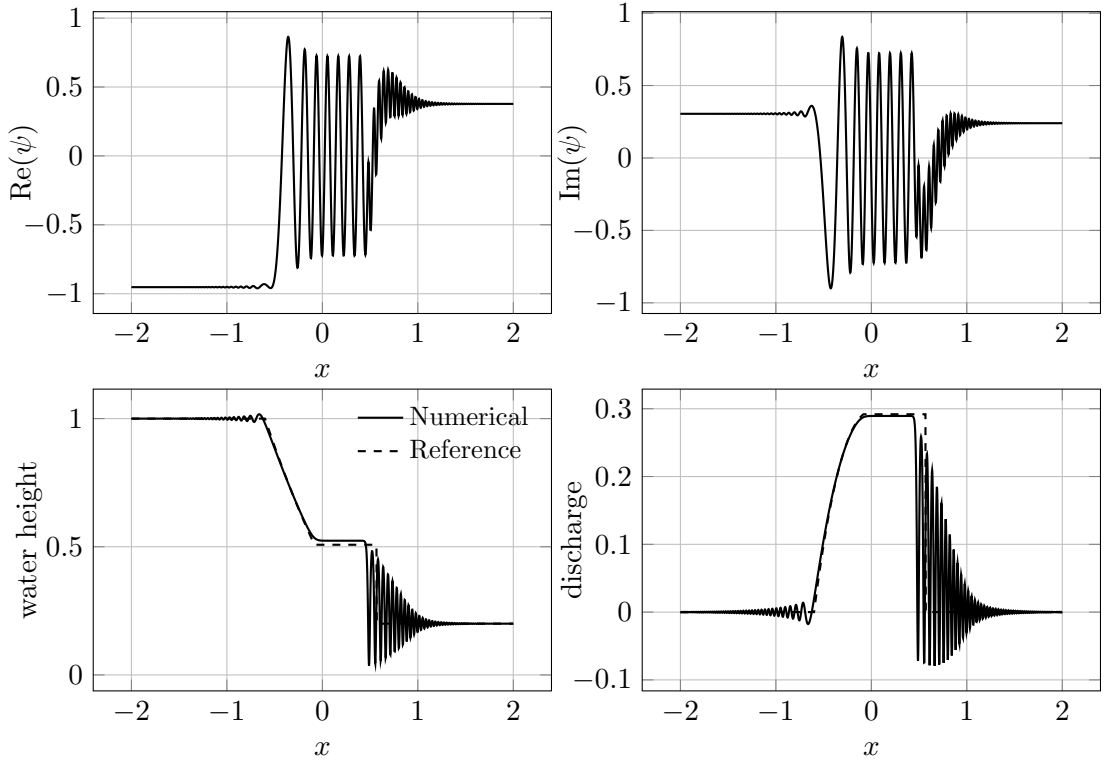


FIGURE 2. Numerical solution of the dam-break problem with a wet bed described in Subsection 3.1.2. The top row shows the real and imaginary parts of the Schrödinger wave function ψ . The bottom row displays the reconstructed hydrodynamic variables, namely the water height $h = |\psi|^2$ and the discharge $q = \varepsilon \operatorname{Im}(\bar{\psi} \psi_x)$. The numerical solutions are compared with the corresponding dispersionless shallow water Riemann solution.

3.1.3. *Generation of Vacuum from Wet Initial States.* Finally, we consider a Riemann problem in which vacuum is generated dynamically. The initial states are

$$(h_L, u_L) = (1.0, -3.0), \quad (h_R, u_R) = (2.0, 3.0).$$

Since

$$2(a_L + a_R) < u_R - u_L, \quad a_L = \sqrt{gh_L}, \quad a_R = \sqrt{gh_R},$$

two rarefaction waves propagate outward, creating an expanding dry region between them. The exact solution contains a vacuum state and is known analytically [24].

Because the initial velocity is nonzero, we employ the sponge-layer boundary treatment described in Subsection 2.6. The computational domain is extended to $\Omega_{\text{ext}} = [-(L + \ell), L + \ell]$ with $L = 2$ and $\ell = 16(2\pi\varepsilon/3) \approx 0.335$.

Figure 3 shows the numerical solution of the vacuum generation problem at the final time $t = 0.3$. As in the previous examples, the Schrödinger wave function exhibits highly oscillatory behavior. In particular, strong oscillations are observed near the left and right far-field regions, where the amplitude approaches constant states and the phase of the wave function varies rapidly. At the scale of the full domain, these oscillations are too rapid to be resolved visually and therefore appear saturated in the plots of $\operatorname{Re}(\psi)$ and $\operatorname{Im}(\psi)$.

Despite this highly oscillatory behavior at the level of the wave function, the reconstructed hydrodynamic variables remain well behaved. Both the water height and the discharge are smooth across the rarefaction waves and accurately capture the formation of the central dry

region. In particular, the numerical solution agrees very well with the dispersionless shallow water Riemann solution.

Small-amplitude oscillations of order $\mathcal{O}(\varepsilon)$ are visible in the reconstructed variables near the edges of the rarefaction fans. These oscillations are consistent with dispersive effects introduced by the Schrödinger regularization and diminish as ε decreases. Overall, this example further demonstrates that, although the Schrödinger wave function itself is highly oscillatory, the Schrödinger-based formulation provides an accurate approximation of the shallow water dynamics in regimes where the solution remains free of shock formation, including cases where a vacuum state emerges dynamically.

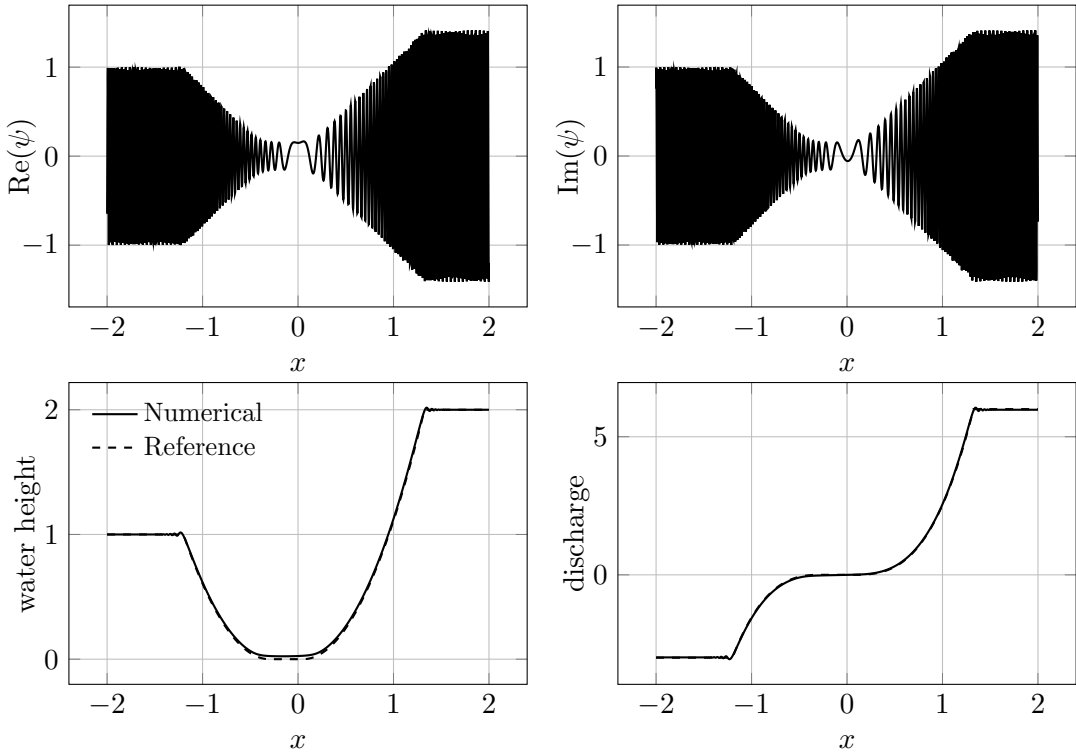


FIGURE 3. Numerical solution of the vacuum generation problem described in Subsection 3.1.3. The top row shows the real and imaginary parts of the Schrödinger wave function ψ . The bottom row displays the reconstructed hydrodynamic variables, namely the water height $h = |\psi|^2$ and the discharge $q = \varepsilon \operatorname{Im}(\bar{\psi} \psi_x)$. The numerical solutions are compared with the corresponding dispersionless shallow water Riemann solution.

3.2. Oscillating lake problem over a parabolic bowl. We next consider the classical oscillating lake problem over a parabolic bowl topography [22, 23], formulated here in a nondimensionalized setting. The bottom topography is given by

$$b(x) = x^2,$$

with initial free-surface elevation, water height, and velocity

$$\eta_0(x) = \max\{0.5 - \sqrt{2}x, b(x)\}, \quad h_0(x) = \eta_0(x) - b(x), \quad u_0(x) = 0.$$

This problem admits an exact periodic solution with moving wetting–drying interfaces,

$$h(x, t) = \eta(x, t) - b(x),$$

where

$$\eta(x, t) = \max\{0.75 - 0.25 \cos(2\sqrt{2}t) - \sqrt{2}x \cos(\sqrt{2}t), b(x)\}.$$

The computational domain is taken as $\Omega = [-2, 2]$, equipped with homogeneous Neumann boundary conditions. The initial Schrödinger wave function is constructed from a regularized

free surface profile,

$$\psi(x, 0) = \sqrt{\delta \log \left(1 + \exp \left(\frac{\eta_0(x) - b(x)}{\delta} \right) \right)}, \quad \delta = 1.2 \varepsilon.$$

Figure 4 presents the numerical solution at times $t = 2.0$, $t = 3.0$, and $t = 4.0$. As in the previous examples, the real and imaginary parts of the Schrödinger wave function exhibit rapidly oscillatory behavior in the small- ε regime. We observe that the oscillation frequency varies with time, reflecting the time-dependent phase structure of the underlying wave function.

Despite these pronounced oscillations at the level of the wave function, the reconstructed free-surface elevation remains smooth and closely follows the exact solution of the dispersionless shallow water equations. In particular, the numerical solution accurately captures the periodic motion of the free surface as well as the evolution of the wetting–drying interfaces. This example further indicates that the Schrödinger-based formulation is applicable to this setting and is able to capture the evolution of wetting–drying interfaces without requiring any ad hoc numerical treatment near dry regions.

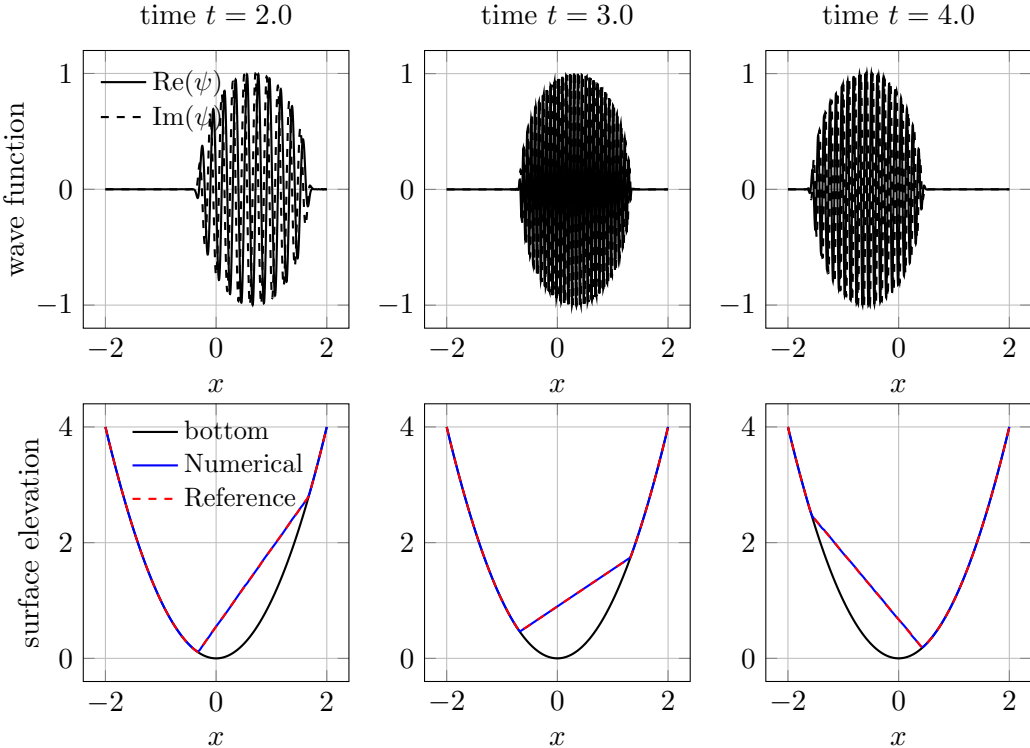


FIGURE 4. Numerical solution of the oscillating lake problem described in Subsection 3.2. The top row shows the real and imaginary parts of the Schrödinger wave function ψ . The bottom row displays the reconstructed free-surface elevation $\eta(x) = h(x) + b(x)$, together with the bottom topography $b(x)$. The left, middle, and right columns correspond to times $t = 2.0$, $t = 3.0$, and $t = 4.0$, respectively.

3.3. Well-Balanced Tests. Finally, we examine the well-balanced behavior of the Schrödinger-based approximation for steady lake-at-rest configurations. We consider the bottom topography

$$b(x) = b_{\max} e^{-10x^2},$$

with initial water height and velocity

$$h_0(x) = (1 - b(x))_+, \quad u_0(x) = 0.$$

The corresponding exact solution of the dispersionless shallow water equations is the steady lake-at-rest state

$$h(x, t) = (1 - b(x))_+, \quad u(x, t) = 0.$$

We impose periodic boundary conditions on $\Omega = [-2, 2]$ and consider two representative cases: $b_{\max} = 0.9$, which corresponds to a fully wet steady state, and $b_{\max} = 1.1$, which produces a partially dry configuration. Numerical results at the final time $t = 1.0$ are shown in Figure 5.

In contrast to the previous test cases, the Schrödinger wave function exhibits significantly reduced oscillatory behavior in this setting. This is consistent with the fact that the underlying shallow water solution is a steady state with zero velocity, so that no rapidly varying phase is generated in the Schrödinger formulation. As a result, the real and imaginary parts of ψ remain relatively smooth in both the fully wet and partially dry cases.

Small deviations from the exact steady free-surface elevation are nevertheless observed in the numerical solution. In both cases, these deviations are of magnitude $\mathcal{O}(\varepsilon)$, reflecting the fact that the nonlinear Schrödinger equation (7) does not satisfy an exact well-balanced property. We also observe that the partially dry configuration exhibits slightly larger approximation errors than the fully wet case, although the overall error level remains of order $\mathcal{O}(\varepsilon)$ in both settings.

4. CONCLUSION

We have introduced a Schrödinger-based dispersive regularization framework for the numerical simulation of the one-dimensional shallow water equations. By solving a semilinear complex-valued Schrödinger equation and recovering the hydrodynamic variables through post-processing, the proposed approach transforms the original nonlinear hyperbolic system into a form that can be efficiently approximated using time-splitting and high-order spatial discretizations. A key advantage of this formulation is its ability to naturally accommodate vacuum states and moving wetting–drying interfaces without requiring ad hoc numerical treatments.

Numerical experiments demonstrate that, in subcritical and shock-free regimes, the Schrödinger-based approximation provides an accurate representation of the dispersionless shallow water solution, with errors typically of order $\mathcal{O}(\varepsilon)$. This includes challenging scenarios involving wetting and drying, vacuum generation, and time-dependent free-surface motion over nontrivial bathymetry. In contrast, when shock formation occurs in the shallow water equations, the Schrödinger regularization produces dispersive shock waves rather than classical entropy shocks, highlighting an inherent limitation of the present approach in such regimes.

Overall, the results indicate that Schrödinger-based dispersive regularization offers a promising alternative framework for the numerical simulation of shallow water flows in regimes where solutions remain smooth or feature vacuum and moving shorelines. Future work will focus on rigorous error analysis in the presence of vacuum, extensions to higher-dimensional settings, and applications to more realistic geophysical and engineering flow problems.

REFERENCES

- [1] Georgios D. Akrivis, Vassilios A. Dougalis, Ohannes A. Karakashian, and William R. McKinney. Galerkin–finite element methods for the nonlinear Schrödinger equation. In *Hellenic research in mathematics and informatics '92 (Athens, 1992)*, pages 421–442. Hellenic Math. Soc., Athens, 1992.
- [2] Robert Anderson, Julian Andrej, Andrew Barker, Jamie Bramwell, Jean-Sylvain Camier, Jakub Cerveny, Veselin Dobrev, Yohann Dudouit, Aaron Fisher, Tzanio Kolev, Will Pazner, Mark Stowell, Vladimir Tomov, Ido Akkerman, Johann Dahm, David Medina, and Stefano Zampini. MFEM: A modular finite element methods library. *Computers & Mathematics with Applications*, 81:42–74, 2021. Development and Application of Open-source Software for Problems with Numerical PDEs.
- [3] Emmanuel Audusse, Fran^{çois} Bouchut, Marie-Odile Bristeau, Rupert Klein, and Beno^{it} Perthame. A fast and stable well-balanced scheme with hydrostatic reconstruction for shallow water flows. *SIAM J. Sci. Comput.*, 25(6):2050–2065, 2004.
- [4] Weizhu Bao and Yongyong Cai. Mathematical theory and numerical methods for Bose-Einstein condensation. *Kinet. Relat. Models*, 6(1):1–135, 2013.
- [5] Weizhu Bao, Shi Jin, and Peter A. Markowich. On time-splitting spectral approximations for the Schrödinger equation in the semiclassical regime. *J. Comput. Phys.*, 175(2):487–524, 2002.
- [6] Weizhu Bao, Shi Jin, and Peter A. Markowich. Numerical study of time-splitting spectral discretizations of nonlinear Schrödinger equations in the semiclassical regimes. *SIAM J. Sci. Comput.*, 25(1):27–64, 2003.
- [7] Shintaro Bunya, Ethan J. Kubatko, Joannes J. Westerink, and Clint Dawson. A wetting and drying treatment for the Runge-Kutta discontinuous Galerkin solution to the shallow water equations. *Comput. Methods Appl. Mech. Engrg.*, 198(17–20):1548–1562, 2009.

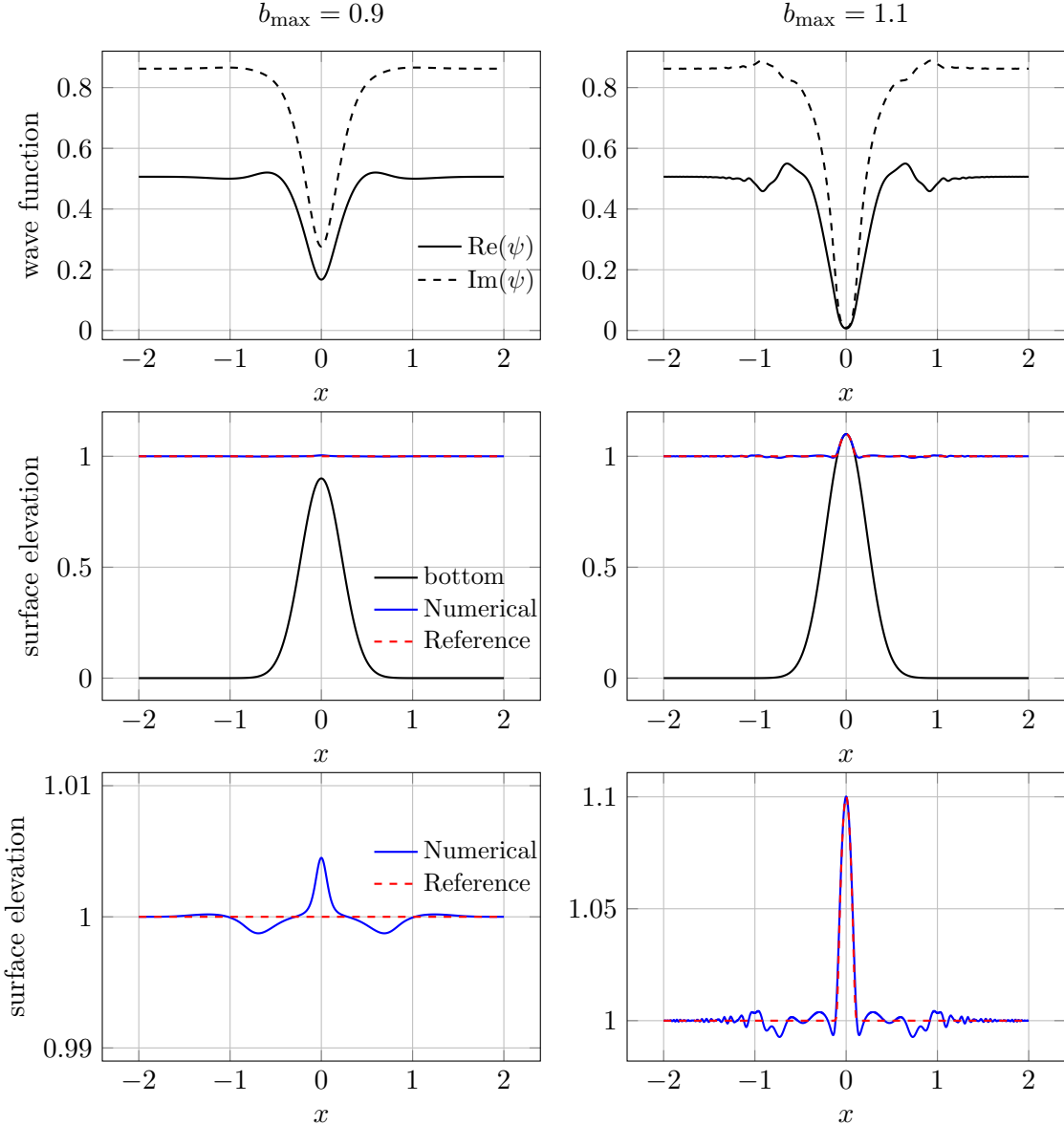


FIGURE 5. Numerical solution at time $t = 1.0$ of the well-balanced problems described in Subsection 3.3. The top row shows the real and imaginary parts of the Schrödinger wave function ψ . The middle row displays the reconstructed free-surface elevation $\eta(x) = h(x) + b(x)$, where $h = |\psi|^2$, together with the bottom topography $b(x)$. The bottom row shows the reconstructed free-surface elevation $\eta(x) = h(x) + b(x)$ without the bottom topography, in order to highlight the small deviations of the numerical solution from the exact (dispersionless) steady state. The left column corresponds to the fully wet case with $b_{\max} = 0.9$, while the right column corresponds to the partially dry case with $b_{\max} = 1.1$.

- [8] Rémi Carles. *Semi-classical analysis for nonlinear Schrödinger equations—WKB analysis, focal points, coherent states*. World Scientific Publishing Co., Singapore, second edition, [2021] ©2021.
- [9] Rémi Carles, Raphaël Danchin, and Jean-Claude Saut. Madelung, Gross-Pitaevskii and Korteweg. *Nonlinearity*, 25(10):2843–2873, 2012.
- [10] Yongxin Chen, Tryphon T. Georgiou, and Michele Pavon. On the relation between optimal transport and Schrödinger bridges: a stochastic control viewpoint. *J. Optim. Theory Appl.*, 169(2):671–691, 2016.
- [11] G. A. El and M. A. Hoefer. Dispersive shock waves and modulation theory. *Phys. D*, 333:11–65, 2016.
- [12] Mi-Ho Giga, Arkadz Kirshtein, and Chun Liu. Variational modeling and complex fluids. In *Handbook of mathematical analysis in mechanics of viscous fluids*, pages 73–113. Springer, Cham, 2018.

- [13] E. Grenier. Semiclassical limit of the nonlinear Schrödinger equation in small time. *Proc. Amer. Math. Soc.*, 126(2):523–530, 1998.
- [14] Li Guo and Yan Xu. Energy conserving local discontinuous Galerkin methods for the nonlinear Schrödinger equation with wave operator. *J. Sci. Comput.*, 65(2):622–647, 2015.
- [15] M. A. Hoefer, M. J. Ablowitz, I. Coddington, E. A. Cornell, P. Engels, and V. Schweikhard. Dispersive and classical shock waves in Bose-Einstein condensates and gas dynamics. *Phys. Rev. A*, 74:023623, Aug 2006.
- [16] Peter D. Lax and C. David Levermore. The small dispersion limit of the Korteweg-de Vries equation. I. *Comm. Pure Appl. Math.*, 36(3):253–290, 1983.
- [17] Christian Léonard. A survey of the Schrödinger problem and some of its connections with optimal transport. *Discrete Contin. Dyn. Syst.*, 34(4):1533–1574, 2014.
- [18] Randall J. LeVeque. *Finite volume methods for hyperbolic problems*. Cambridge Texts in Applied Mathematics. Cambridge University Press, Cambridge, 2002.
- [19] Chun Liu. An introduction of elastic complex fluids: an energetic variational approach. In *Multi-Scale Phenomena in Complex Fluids: Modeling, Analysis and Numerical Simulation*, pages 286–337. World Scientific, 2009.
- [20] E. Madelung. Quantentheorie in hydrodynamischer form. *Zeitschrift für Physik*, 40:322–326, 1927.
- [21] Peter A. Markowich, Paola Pietra, Carsten Pohl, and Hans Peter Stimming. A Wigner-measure analysis of the Dufort-Frankel scheme for the Schrödinger equation. *SIAM J. Numer. Anal.*, 40(4):1281–1310, 2002.
- [22] Joe Sampson, Alan Easton, and Manmohan Singh. Moving boundary shallow water flow above parabolic bottom topography. *ANZIAM J.*, 47:C373–C387, 2005.
- [23] William Carlisle Thacker. Some exact solutions to the nonlinear shallow-water wave equations. *J. Fluid Mech.*, 107:499–508, 1981.
- [24] Eleuterio F. Toro. *Computational Algorithms for Shallow Water Equations*. Springer, Cham, Switzerland, 2nd edition, 2024.
- [25] G. B. Whitham. *Linear and nonlinear waves*. Pure and Applied Mathematics. Wiley-Interscience [John Wiley & Sons], New York-London-Sydney, 1974.
- [26] Yulong Xing and Chi-Wang Shu. High-order finite volume weno schemes for the shallow water equations with dry states. *Advances in Water Resources*, 34(8):1026–1038, 2011.
- [27] Yulong Xing and Xiangxiong Zhang. Positivity-preserving well-balanced discontinuous Galerkin methods for the shallow water equations on unstructured triangular meshes. *J. Sci. Comput.*, 57(1):19–41, 2013.

DEPARTMENT OF APPLIED AND COMPUTATIONAL MATHEMATICS AND STATISTICS, UNIVERSITY OF NOTRE DAME, USA.

Email address: gfu@nd.edu

DEPARTMENT OF APPLIED MATHEMATICS, ILLINOIS INSTITUTE OF TECHNOLOGY, USA.

Email address: cliu124@iit.edu